Flow Visualization and Flow Field Measurements of a 1/12 Scale Tilt Rotor Aircraft in Hover

Charles D. Coffen
Graduate Research Assistant
Cornell University
Ithaca, NY

Albert R. George
Professor
Cornell University
Ithaca, NY

Hal Hardinge
Graduate Student
Cornell University
Ithaca, NY

Ryan Stevenson
Undergraduate Research Assistant
Cornell University
Ithaca, NY

ABSTRACT

This paper details the results of flow visualization studies and inflow velocity field measurements performed on a 1/12 scale model of the XV-15 tilt rotor aircraft in the hover mode. The complex recirculating flow due to the rotor-wake-body interactions characteristic of tilt rotors was studied visually using neutrally buoyant soap bubbles and quantitatively using hot wire anemometry. Still and video photography were used to record the flow patterns. Analysis of the photos and video has provided information on the physical dimensions of the recirculating fountain flow and on details of the flow including the relative unsteadiness and turbulence characteristics of the flow. Recirculating flows were also observed along the length of the fuselage. Hot wire anemometry results indicate that the wing under the rotor acts to obstruct the inflow causing a deficit in the inflow velocities over the inboard region of the model. Hot wire anemometry also shows that the turbulence intensities in the inflow are much higher in the recirculating fountain re-ingestion zone.

INTRODUCTION

Tilt rotor aircraft have several novel features which affect their aerodynamic characteristics. In various flight modes the rotor and rotor-wake-body aerodynamics are different from either helicopters or conventional aircraft. In the operation of a tilt rotor aircraft in hover, the presence of the wing and fuselage beneath the rotor affects the aerodynamics by introducing complex unsteady recirculating flows.

The fundamental geometry of the tilt rotor aircraft (Figure 1 picture of aircraft) consists of prop-rotors mounted on tiltable nacelles which are located at or near the tips of a fixed (non-tilting) wing. The prop-rotor is sufficiently large so that the benefits of low disk loading are gained for efficient hover flight. The prop-rotor is designed to provide the desired performance balance between the axial-flow critical hover requirement and the axial-flow airplane mode requirement[1,2,3]. The tilt rotor introduces a number of unique prop-rotor/airframe aerodynamic interactions that must be addressed to properly

understand the significant performance issues. In hover mode the wing and fuselage provide a partial ground plane in the near wake which causes the development of an inboard-bound spanwise flow over the wing and fuselage surface. At the aircraft's longitudinal plane of symmetry, the opposing flows collide, producing a low energy fountain flow with upward velocity components which are then re-ingested by the rotors. Full analytical representation of this flow would require a three-dimensional, time-variant, rotor/rotor, and rotor-airframe interaction model.

Some characteristics of tilt rotor flow have been studied both experimentally and analytically. Experimental tests on large and full scale models have been used to study the down load on the wing in the hover condition[4,5,6,7,8]. This problem is of great interest as 10%-15% of the rotor lift is needed to overcome the down force on the wing caused by the down wash flow over the wing. All of these tests used one wing and rotor and an image plane rather than a complete mock up. According to the study by Felker and Light[8] the size of the image plane can have a profound effect on the test results. One previous experimental study of the tilt rotor hover condition not limited to downwash and down loads was by Rutherford[9]. In this test smoke and tuft flow visualization techniques were used on a model consisting of a single wing and rotor. An image plane was used to simulate the two rotor-wing flow phenomena.

The study of reference (10) attempts to analytically study the flow of a tilt rotor XV-15 in hover by numerically solving the unsteady, thin layer compressible Navier-Stokes Equation. While the results of this study are encouraging, not all the major features of tilt rotor hover flow are captured in the computation. In particular, this study included only a wing and rotor image system in the calculation. Attempts at modeling tilt rotor hover flow by assuming a plane of symmetry and disregarding the fuselage will be shown here to be insufficient.

While a full analytical representation may be desirable in the long term, a more expedient method is required for generating data needed for current aerodynamic and aeroacoustic calculations and design. Thus a 1/12 scale model (consisting of two rotors, wing, and fuselage) of the XV-15 tilt rotor was built in order to qualify and quantify the complex flows about a hovering tilt rotor. This model enables the study of the unsteadiness and ths side to side shifting of both the fountain flow which have not been previously explored. Prior tests have relied on an image plane to simulate the tilt rotor hover configuration. Past experimental tests have also not included the fuselage which also affects the overall flow. Important flow phenomenon were found to occur along and above the length of the fuselage. In addition, attempts to model the flow analytically require accurate and complete experimental information for comparison and validation. Previous tests have not been adequate in this respect.

This study provides a more thorough understanding of the qualitative and quantitative characteristics of the recirculating flow, such as relative turbulence levels, unsteadiness in the flow and the three dimensional nature of the fountain flow. The results of this study will serve as a comparison for CFD calculations and design modifications.

EXPERIMENTAL SETUP

The scale of the model was determined by the size of the largest commercially available propeller, 24 inch diameter with a pitch of 8 inches. Electric motors were chosen to power the model. No attempt was made to Mach scale the rotor tip speed. As the rotor pitch was scaled approximately, the ratio of tip speed to induced velocity will be approximately scaled. Most fixed speed electric motors operate at either 1700 or 3450 rpm. In order to obtain higher inflow velocities (less relative error for the measuring equipment available), a motor speed of 3450 rpm was chosen. Two 1.5 hp motors operating at 3450 rpm were used. The motors were uncoupled as coupled motors would have been difficult to implement and maintain. The uncoupled motors were operated at the same speed by controlling one motor's speed with a variac and matching speeds with a stroboscope. We do not expect that the lack of phase locking between the rotors will be significant as the rotor tip speed is much greater than the induced velocity giving many tip vortices and associated wake structures per unit axial length. The motors spin in opposite directions so that the blades

rotate towards the tail as they pass over the wing. The motors are located approximately 7 inches below the wing, far enough below the rotors to be out of the flow yet not so far as to make shaft whirl a problem.

The wing and fuselage were both constructed using a styrofoam base covered with fiberglass, filler and paint. The horizontal and vertical tail were not installed in the tests reported here. The wing is removeable and has adjustable flaps and flaperons to allow for testing of various wing configurations. The model is mounted on a steel frame to oppose the lift of the rotors and reduce vibration. The model is supported by a wooden structure elevated above the floor such that the rotor plane is 60.75 inches above the ground. This corresponds to a hover height of 60.75 scale feet. Figure (2) shows the the experimental set up including the model, electric motors and test stand. The model was operated in an area of dimensions greater than 25 feet. The nearest significant objects in the room were approximately 10 feet away. The orientation and placement of the model in the room was found not to affect the observed and measured flow.

FLOW VISUALIZATION

A very effective tool for visualizing the complex flows of the model XV-15 was a bubble generator. The Model 3 Sage Action Incorporated Bubble Generator combines compressed air, helium, and a soap solution to produce neutrally-buoyant helium filled bubbles[11]. The bubbles follow the pathlines of the flow and are able to accurately trace the intricate flow patterns of the hovering tilt rotor. Rubber tubing and an aluminum tube wand were used to insert the bubble at various locations in the flow. During the experiment, the room was darkened and a high intensity Varian arc lamp was used to illuminate the bubbles.

Results of Still Photographs:

The flow around a hovering tilt rotor is extremely unsteady. Still photographs were used to capture various features of the flow. It must be noted that these are instantaneous visualizations. ASA 1600 film was used with an f-stop of 5.6 and 0.25 to 1.0 second exposure times. Greater exposure times produced pictures with too many 'cluttered' pathlines and smaller exposure times did not allow enough light. Still photographs were taken of the front and side of the model. Unless otherwise obvious, the bubbles were inserted in the longitudinal plane of symmetry. In order to view a two dimension slice of the the flow patterns, the light source was situated perpendicular to the direction of the camera.

Figure (3) is a top view schematic of the model and indicates the aircraft axis and indicates probe locations for the various experiments.

The images presented here are computer enhancements of the original stills which were digitized using a scanner. Figure (4) shows an unenhanced photo. Figure (5) is the same photo which has been inverted (negative image) to show the pathlines as black streaks on a white background. The contrast of the scanned images was improved to better define the bubble streaks. This process often caused a blurring of the model with the background. Also, light reflected off the model caused distracting shadows and in many cases obliterated the outline of the model. In order to reduce this annoying affect, the outline of the model was enhanced and the background edited to clarify the image and remove distracting shadows. In no cases were the bubble streaks or any part of the flow embellished or manipulated.

Figure (5) is a head on photo of the model with the bubbles being injected directly over the intersection of the longitudinal axis and the rotor/rotor axis. This figure clearly shows the recirculating fountain and indicates the height of the fountain to be approximately 1/2 the radius of the rotor. This figure also shows an unsteady stagnation point on the fuselage where the spanwise flows intersect and erupt up between the two rotors and are then re-ingested. Figure (6) emphasizes the re-ingestion part of the flow as bubbles inserted just above the unsteady stagnation point are convected up between the rotors where they are entrained into the induced flow and are re-ingested. Figure (7) indicates the extremely turbulent nature of the fountain flow near the unsteady stagnation point. Here bubbles are injected horizontally along the longitudinal axis. The random direction of the pathlines, the sharp lateral perturbations, and the fact that the bubbles are injected at the same location in the flow and follow completely dissimilar paths, all indicate the highly unsteady and turbulent nature

of the fountain flow. Note that all of these images project the 3-D flow onto a plane and that information about the flow out of the plane is lost. Figure (8) shows bubbles being injected off center and shows the spanwise flow curling up before reaching the longitudinal axis. This figure also shows one bubble being convected from the center of the fountain into the interior of the rotor disk and another being convected into the opposite rotor. Presumably these events are due to particularly large turbulent eddies being ingested.

The next four Figures (9-12) illustrate the fountain flow from the side and clearly illustrate the multi-dimensional nature of the recirculating fountain flow. These aspects of the flow are difficult to explain as the images show several recirculation paths. Note that the model used in this study did not include a tail wing assembly which may have some minor influence on the fountain flow over the rear of the fuselage.

The pathlines of the bubbles over the rear of the fuselage depend strongly on their point of injection. Figure (9) shows bubbles being injected above the tail, over the longitudinal axis, and above the rotor plane. The bubbles are swept horizontally along the longitudinal axis and are ingested into the rotors to both sides of the upflow shown in Figure (5). The bubbles pass through the rotor plane and travel back towards the tail along the fuselage. Here the bubbles recirculate upward above the rotor plane and are eventually re-ingested. Figure (10) shows the bubbles being injected along the fuselage near the tail. This photo differs from the one above in that the bubbles are injected below the rotor plane. The bubbles are lifted off the fuselage and are entrained in the recirculating flow along and above the fuselage. The next Figure (11) shows what happens when bubbles are injected over the wing, over the longitudinal axis, and below the the rotor. This probe placement is similar to that of Figure (6) but the photo is from a different view. Here the bubbles are convected up between the rotors and are dispersed rearward and to one or the other side of the fuselage where they are re-ingested. Figure (12) demonstrates how the near laminar inflow becomes distorted and erratic as it interracts with the recirculating fountain flow over the fuselage. Unlike the coherent flow structures provided by the head on photos, these images do not indicate any distinct flow pattern which can be said to characterize the flow above the fuselage. Most likely, the entire region from the wing/fuselage intersection rearward on the fuselage represents an unsteady stagnation zone. This flow is characterized by low velocity highly turbulent flow. The flow along the fuselage tends to be entrained up between the two rotors and re-ingested through the rotors in a cyclical process. The pathlines are dependent on the point of origin, but it appears that bubbles injected anywhere above the fuselage will eventually enter this stagnation zone and become re-ingested.

The most important conclusion that can be drawn from these photos is that the fountain is not a phenomenon which can be viewed or analyzed in two dimensions. This flow is multi-directional and includes spanwise flow along the wings and unsteady flow along the fuselage. Both of these components exhibit turbulent upward flow paths which result in re-ingestion of the flow.

Results of Video Recording:

In order to record the strong time dependence of the flow, video recordings of the bubble pathlines were also made. Bubbles were inserted in various places in the flow to show various pathlines. The location of insertion point is very important for visualizing different flow phenomenon. One important feature of the video recordings is the availability of slow motion and frame-by-frame advance. The downwash velocities are fast enough to make it difficult for the human eye to see all there is to see in the video at standard speeds. The frame-by-frame advance shows 0.04 second intervals. Between frames, the pathlines disappear and new pathlines appear as bubbles move in and out of the stream of light. This demonstrates the gross unsteadiness in the flow and demonstrates the 3-dimensional nature of the flow. This is an important point because the recorded images show the fountain flow superimposed on a 2D plane. In fact, the fountain flow is omni-directional and must be studied from all angles in order to fully appreciate the complexity of the flow.

Another important phenomenon of the flow documented with video was the side-to-side switching of the fountain. This effect is most apparent when the model is viewed head on and

bubbles are injected above the rotor plane. The recirculating flow is seen to switch randomly from side to side in time. The time scale of this phenomenon was measured to be anywhere from 0.04 seconds or less (frame advance time) to 0.75 seconds. The fluctuation is characterized by the fountain flow being re-ingested mostly into one of the two rotors. This switching indicates the unsteadiness of the stagnation region on and above the fuselage. The asymmetry of this phenomenon shows that modeling the fountain flow with one rotor and an image plane is inadequate for studying the time varying properties of the flow.

HOT WIRE EXPERIMENTS

Hot wire anemometry was another technique used to help characterize the fountain flow. These experiments were conducted with a single wire probe. Unless otherwise indicated, the wire was parallel to the plane of the rotor and was oriented parallel to the longitudinal axis. The anemometer was connected to a Macintosh based data acquisition system. Three experiments are reported. The first experiment was an attempt to characterize the unsteadiness of the flow by examining time traces of velocity measurements. For these measurements, a sampling rate of 4000 samples per second for one second was used. Another experiment was to measure the spectrum of turbulence due to the recirculating fountain. For this experiment the sampling rate was 30,000 samples per second. 2^{14} evenly spaced samples were used to find the spectrum. The last experiment was an attempt to quantify the mean and rms inflow velocities over the rotor plane. The mean velocity spatial variations are affected by the wing obstructing the rotor wake, and the rms velocity spatial variations are affected by the re-ingestion of the fountain turbulence. 625 locations one inch above the rotor plane were measured. A sampling rate of 40 samples per second for 15 seconds was used.

Time Traces:

The unsteadiness of the location and turbulent intensity of the fountain flow is evident from time traces of velocity at various points in the flow. Figure (13a-b) compare two 0.13 second time series of inflow velocity measured 2 inches from the tip on the rotor/rotor axis and one inch above the rotor plane (in the fountain re-ingestion zone of the rotor). Refer to Figure (3) for a schematic of the model and measurement locations. Based on the results of the flow visualization study, this location was chosen as a reference point because it is more or less centered in the re-ingestion area. These series show how the inflow can be either laminar, essentially showing only the blade passing, Figure (13a), or very turbulent, Figure (13b), due to re-ingestion of the wake. Figure (14) gives an example of the intermittency of the phenomenon as this sample shows a nearly laminar inflow broken by a 0.05 second burst of turbulence followed by a return to laminar flow. A study of a 4.0 second series, Figure (15), did not indicate any discernable pattern in the period of intermittency. Figure (16) shows a time trace over the outboard section of the rotor plane, one inch above the rotor and 2 inches from the tip on the rotor/rotor axis. Here the inflow is laminar and is undisturbed by the turbulent fluctuating recirculating fountain flow. Another interesting observation is that the peak inflow velocity due to the potential flow is 2 m/s greater in Figure (16) than in Figure (13a). This result is due to the wing obstructing the flow inboard and will be discussed in more detail below.

The height of the fountain was also studied by taking time traces at 1, 3, and 5 inches above the rotor plane at the point 2 inches inboard of the rotor tip on the rotor/rotor axis (in the fountain re-ingestion zone of the rotor). Figures (17a-c) show the progression of heights. The velocity fluctuations due to the potential flow associated with each blade passage decreases with increasing height. The amplitude of fluctuations due to the re-ingested fountain turbulence decreases from 1 to 3 inches above the rotor plane, but does not decrease as much between 3 and 5 inches above the rotor plane. The fluctuations are more rapid at the 1 and 3 inch heights than the 5 inch height. This indicates that the smaller turbulent eddies are re-ingested at a lower height and that only large scale eddies are recirculated to greater heights above the rotor plane. This result can also be seen in the flow visualization photos as the pathlines become less erratic as they travel higher above the rotor plane. This information may be useful for future attempts to ameliorate the fountain affect by reducing or eliminating its high frequency content.

Velocity versus time traces were also used to study the fountain flow above the fuselage. Figure (18a-e) show series at five locations on the longitudinal axis one inch above the rotor plane. These Figures show how the flow is recirculated preferentially to the rear of the aircraft. The velocity fluctuations fall off drastically as the probe is moved forward of the wing while remaining fairly constant as the probe is moved rearward. Figure (18e) is of special interest as it shows large rapid fluctuations one rotor radius behind the wing/fuselage intersection. This shows that the longitudinal recirculating flow is not a minor or secondary affect and should be studied further as it may effect many operational characteristics such as hover performance, stability, and interior cabin noise.

Time traces were also generated for the case of the hot wire centered between the two rotors over the wing and one inch above the rotor plane with one and both rotors spinning. A comparison of these two half second traces (Figure (19a-b)) shows how the two rotors and wing fuselage create a highly turbulent recirculating flow. The trace with one rotor running, Figure (19a) shows variations corresponding to the blade passage and some very mild disturbances of magnitude less than 1 meter/second due to ambient room turbulence. With both rotors spinning, Figure (19b) the fluctuations have magnitudes as great as 14 m/s which are due to the unsteady turbulent recirculating flow.

Turbulence Spectra:

The time traces described above are meant to provide a more qualitative view of the relative magnitudes and intermittency of the flow components measured by a single hot wire. Another experiment was to quantify the nature of the fountain turbulence. The spectrum of velocity squared was calculated from a stream of velocity measurements from a single hot wire. Figure (20) compares the power spectrum of inflow velocities measured by a single wire probe 1 inch above the rotor plane and 2 inches from the tip on the rotor/rotor axis in the re-ingestion zone. The top curve shows the turbulence due to the re-ingestion of the fountain flow. The lower curve is the power spectrum of the ambient inflow turbulence which was found by taking measurements with only one rotor spinning and the model removed from the experiment. Both spectra show the blade passing harmonics at integer multiples of approximately 113 Hz. This plot shows that there is 5 to 10 times more energy per unit frequency in the fountain turbulence than in the room turbulence for frequencies between 10Hz and 2kHz. This plot also shows that the spectral energy for the two cases becomes the same at frequencies higher than 10kHz. The greater low frequency content of the fountain inflow may be due to the intermittency discussed above while the increased high frequency velocity fluctuations are due to the re-ingestion of the turbulent recirculating fountain flow.

Mean and rms Inflow Velocities:

Mean and rms velocities were also measured on an evenly spaced 25" by 25" square grid 1 inch above the rotor plane. Three grids of data were taken for the three Cartesian orientations of the hot wire. Reduction of this data was complicated by several factors. A fully three dimensional turbulent flow cannot be quantified using a single wire hot wire unless some assumptions are made about the relative magnitudes of the velocity components. Also, the grid of hot wire measurements would have been better oriented in a cylindrical coordinate system as this would best fit the geometry of a hovering rotor. A Cartesian system was used as the only available traverse was not appropriate for moving the probe with respect to radius and azimuthal angle. The data then had to be reduced in cylindrical coordinates. In order to do this, the theta component of mean velocity was assumed to be negligible compared to the radial and axial mean velocities. Another complicating factor was that the data was taken with a single wire probe which meant that data points had to be measured separately for each hot wire orientation. This leaves the possibility for error due to inexact probe placement for each set of measurements. Another source of error is that the rms values of velocity are sometimes more than 20% of the mean velocity which implies that King's Law is less accurate. Future measurements will be conducted with an x-wire.

Figure (21) is a contour plot showing the axial component of mean velocity over the rotor plane. Clearly there is a deficit in the inflow velocity

over the wing. The deficit is recognizeable by lighter shading over the wing and lower valued contours. As has been hypothesized before[12,13] this deficit is due to the wing obstructing the flow beneath the rotor. While these results are not accurate enough to precisely model the fountain flow, they are conclusive in showing this important phenomenon of tilt rotor hover flow.

Figure (22) is a plot of the rms velocity over the rotor plane. This contour plot uses values obtained from three orthogonal sets of hot wire data and plots the values of $\sqrt{V_r'^2 + V_\theta'^2 + V_z'^2}$. No attempt was made to reduce this data to component form for the following reason; While the turbulence is most likely isotropic at higher frequencies, the data was measured 1" above the rotor plane and therefore it also reflects the velocity fluctuations due to the potential flow field (blade passage). Thus we are unable to present the rms velocities by component as we are unable to precisely separate the potential flow velocity fluctuations from the velocity fluctuations due to the inflow turbulence. Qualitatively the existence of the potential flow is not a problem as the turbulent velocity fluctuations in the re-ingestion zone are significantly greater than those caused by the potential flow field. This is apparent from Figure (22) which shows the re-ingestion zone as a region of high rms velocities (darker shading) on the in-board section of the rotor. These high values are a result of the turbulent fountain flow recirculating into the inflow where it is measured as velocity fluctuations by the hot wire. This plot also shows higher rms values towards the rear of the grid which indicates that the flow is re-ingested in the rearward side of the rotor/rotor axis. This region of high rms velocities corresponds to the re-ingestion region observed in the flow visualization study.

Thus, this contour plot of rms velocities shows the high levels of turbulence in the re-ingestion zone of the rotor due to the recirculating fountain. These rms velocities are significantly higher than the rms velocities due to the potential flow. However, the existence of the potential flow field masks the ambient inflow turbulence outside of the re-ingestion zone. Although this obscures the relative magnitudes of the re-ingested turbulence and the ambient turbulence, the significance of the the fountain flow being re-ingested is readily apparent from the high rms velocities over the inboard section of the wing.

SUMMARY AND CONCLUSIONS

1. The recirculating fountain has been studied and recorded in photos and video. This flow phenomenon is easily identified as the opposing spanwise flows meet at an unsteady separation point on the fuselage and erupt over the rotor plane and are re-ingested.

2. Side views of the model indicate that unsteady recirculating flow exists along and above the length of the fuselage. This aspect of the flow was previously unidentified and its characteristics warrant future study.

3. The fountain flow is an multi-directional phenomenon and efforts to study or model the flow in two dimensions will not capture all the important aspects of the flow.

4. The recirculating fountain is strongly time dependent as it tends to randomly shift about the aircraft's longitudinal axis. This causes in intermittency effects which cannot be studied by replacing one side of the model with an image plane.

5. The unsteadiness and intermittency of the fountain flow were observed with velocity time traces obtained using hotwire anemometry. The time traces indicated much more turbulent flow over the rear of the aircraft than over the nose.

6. Turbulence spectra indicate that inflow turbulence in the re-ingestion zone over the rotor contains 5 - 10 time as much energy per unit frequency over a broad range of frequencies than is in the basic inflow turbulence of a single rotor with no fuselage or wing.

7. Contour plots of mean and rms velocities were generated at a height of one inch above the rotor plane. These contours indicate a velocity deficit in the axial component of the inflow velocity in the region over the wing. This deficit is due to the flow obstruction caused by the wing. The contour plot of rms velocity shows high values over part of the

rotor. These high values are due to the highly turbulent flow being re-ingested. Both the inflow velocity deficit region and highly turbulent inflow velocity region are clearly observed on the contour plots.

8. The results of this study are of a semi-quantitative nature. The Reynolds numbers are lower than for the XV-15 aircraft and the rotor blade geometries are not scaled precisely. Some moderate assumptions were needed to reduce the hot wire velocity measurements. Future studies are planned under more rigorous conditions in order to study the details of the flow, further quantify it, and look for methods of altering the flow.

ACKNOWLEDGEMENTS

The authors would like to acknowledge the advice and technical support of Edward Dull and Todd Ringler who are graduate students in the Aero and Acoustic Research Group at Cornell. We also wish to acknowledge the experimental and machine work of undergraduates Darren Halford, Paul Hamill, and John Shatz. The hot wire measurements were obtained with a data aquisition system implemented by Edward Dull and programmed by Mitchell Radisher. Spectral results were obtained using ALDAS, a NASA Ames code prepared by Mike Watts. The flow visualization photographs were digitized and enhanced with the help of Theresa Howely, Illustrator and Technical Specialist. This research was supported by NASA Grant NAG 2-554, the NASA-Cornell Space Grant Program, and the Cornell College of Engineering Undergraduate Research Program supported by Mr. James Moore.

REFERENCES

1. Rosenstein, H., and Clark, R. (1986). "*Aerodynamic Development of the V-22 Tilt Rotor*", AIAA Aircraft Systems, Design and Technology Meeting, October 1983, Paper No. AIAA-86-2678.

2. McVeigh, M. A., Rosenstein,H., and McHugh, F. J. (1983). "*Aerodynamic Design of the XV-15 Advanced Compositie Tilt Rotor Blade*", 39th Annual Forum of the American Helicopter Society, May 1983.

3. Paisley, D. J. (1987). "*Rotor Aerodynamics Optimization for High Speed Tiltrotors*", 43rd Annual Forum of the American Helicopter Society, May 1987.

4. McCroskey, W.J., Spalart, Ph., Laub, G.H., Maisel, M.D., and Maskew, B. "*Airloads on Bluff Bodies, With Application to the Rotor-Induced Downloads on Tiltrotor Aircraft*", Paper No. 11, Ninth Europpean Rotorcraft Forum, September 13-15, 1983.

5. Felker, F. F., Maisel, M. D., Betzina, M. D., "*Full-Scale Tiltrotor Hover Performance*", Proceedings of the 41st Annual Forum of the American Helicopter Society, Fort Worth, Texas, May 1985.

6. McVeigh, M. A., "*The V-22 Tiltrotor Large-Scale Rotor Performance/Wing Download Test and Comparison with Theory*", Proceedings of the 11th European Rotorcraft Forum, London, England, September 1985.

7. Clark, D. R., and McVeigh, M. A., "*Analysis of the Wake Dynamics of a Typical Tiltrotor Configuration in Transition Flight*", Proceedings of the 11th European Rotorcraft Forum, London, England, September 1985.

8. Felker, F. F. and Light, J. S., "*Rotor/Wing Aerodynamic Interactions in Hover*", Proceedings of the 42nd Annual Forum of the American Helicopter Society, Washington, D. C., June 2-4, 1986.

9. Rutherford, J. W., and Morse, H. A. (1985). *The Tilt Rotor Download Investigation*, Videotape, U. S. Army Aeroflightdynamics Laboratory, 7 x 10 Wind Tunnel, Ames Research Center, July 1985.

10. Fejtek, I. and Roberts, L., "*Navier-Stokes Computation of Wing/Rotor Interaction for a Tiltrotor in Hover*", AIAA Paper 91-0707, Proceedings of the 29th Aerospace Sciences Meeting, Reno, Nevada, January 7-10, 1991.

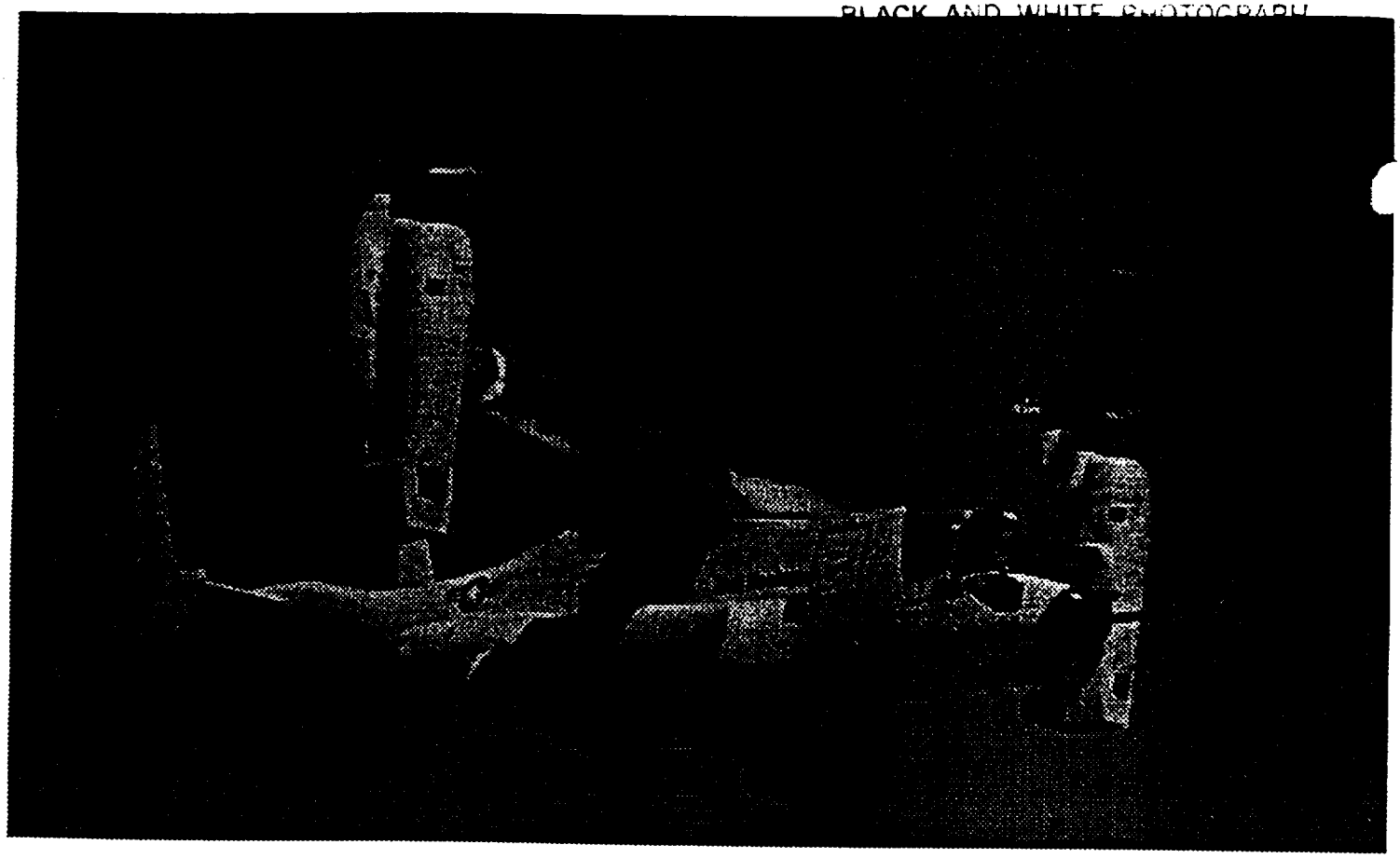

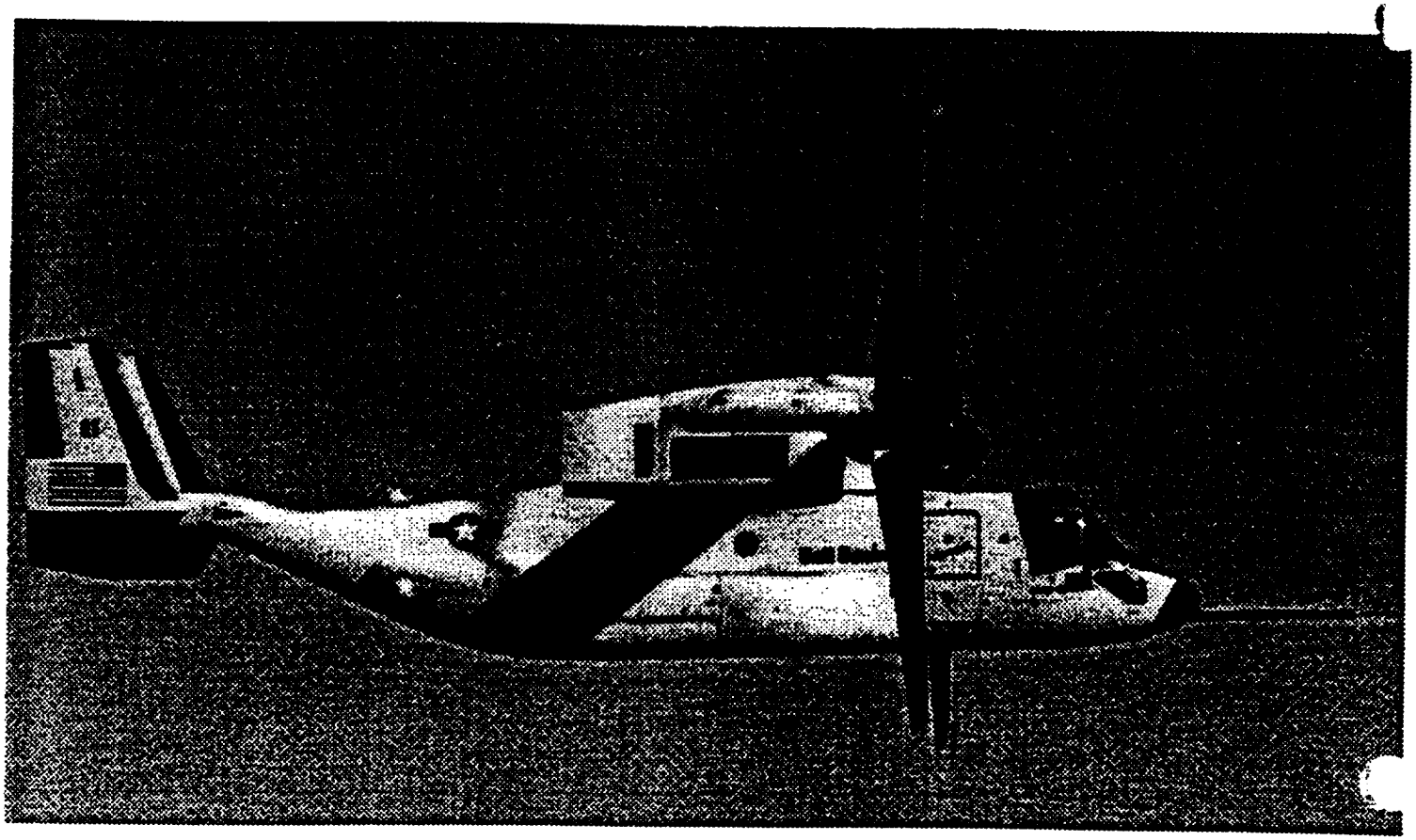

Figure 1. Hover and forward flight configurations for the tilt rotor aircraft.

11. Ordway, D., SAI Bubble Generator: Description and Operating Instructions. Sage Action Inc., Ithaca, New York, March, 1971.

12. George, Albert. R., Smith, Charles A., Maisel, Martin D., and Brieger, John T. (1989). *"Tilt Rotor Aircraft Aeroaacoustics"*, Proceedings of the 45th Annual Forum & Technology Display of the American Helicopter Society, Boston, Massachusetts, May 22-24, 1989.

13 Coffen, C. D., George, A. R., (1990). *"Analysis and Prediction of Tilt Rotor Hover Noise"*. Proceedings of the 46th Annual Forum & Technology Display of the American Helicopter Society, Washington D.C., 1989.

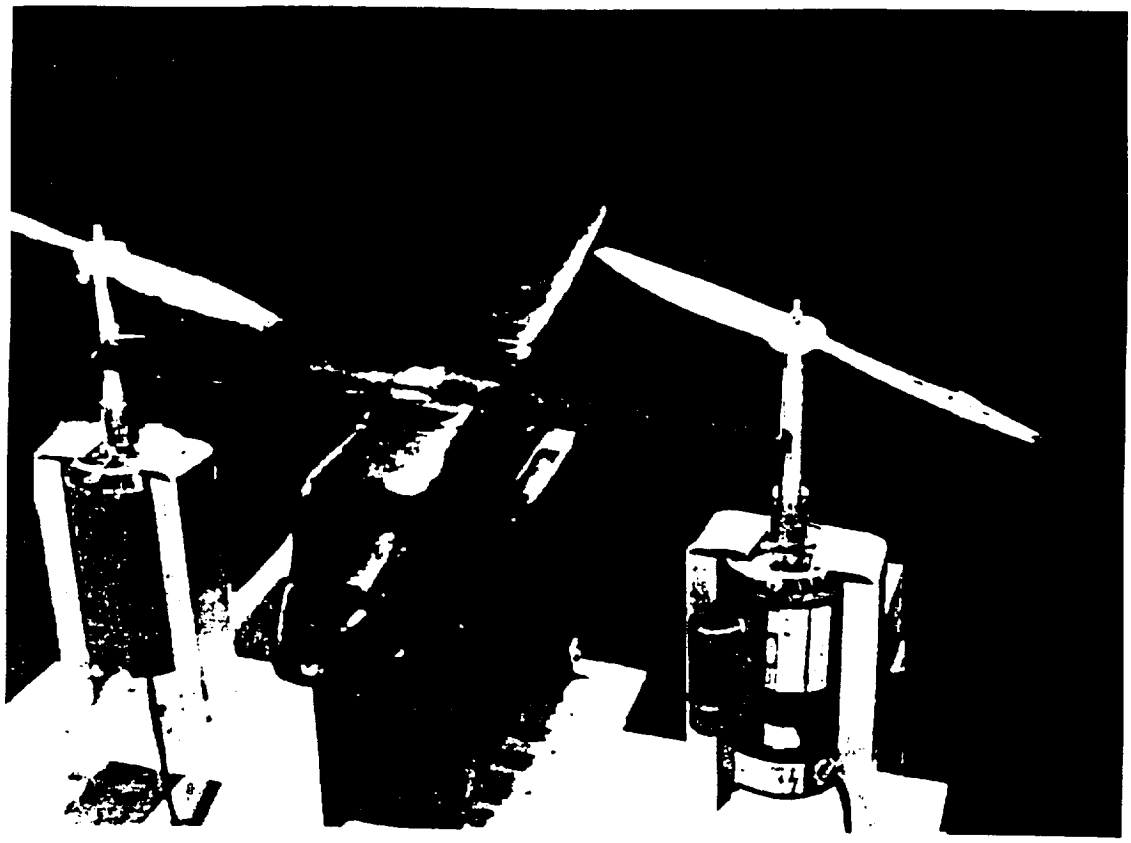

Figure 2. Photo of the 1/12 scale tilt rotor showing model, motors and mounting.

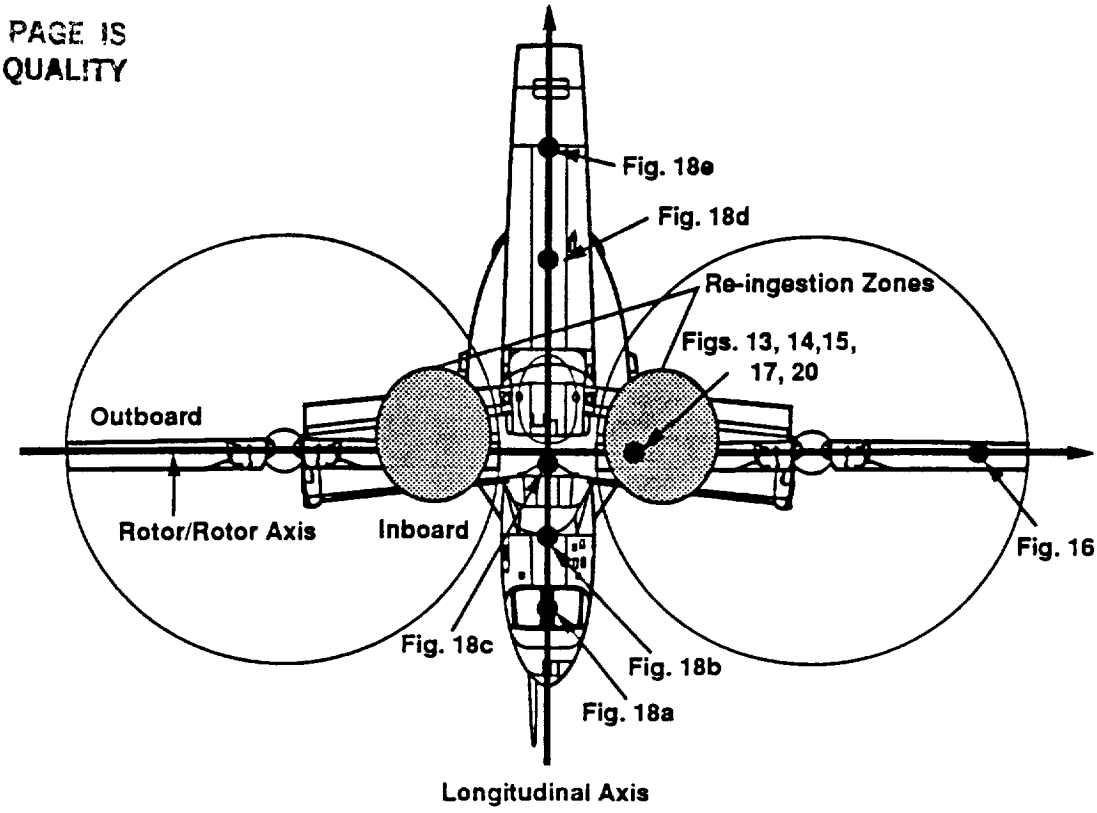

Figure 3. Schematic of model top view showing probe placements, axes, and approximate re-ingestion zones. (Actual. model has 2 blades and no tail for these tests).

Figure 4. Un-enhanced digitized photo of fountain flow. Viewer in front of model. Bubbles are injected over the center of the wing on the rotor/rotor axis. 1/2 second exposure time.

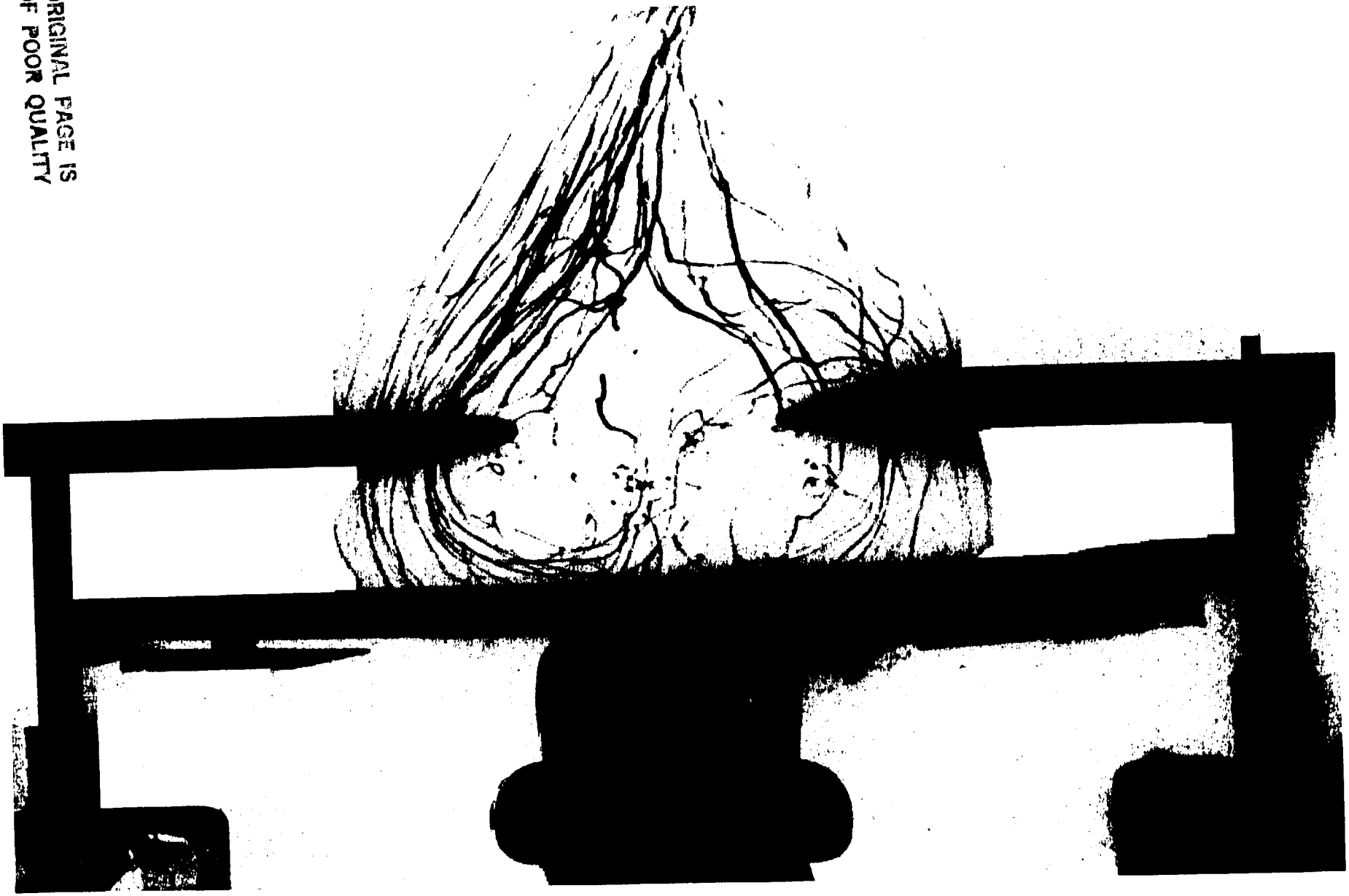

Figure 5. Computer enhanced digitized photo of fountain flow. Viewer in front of model. Bubbles are injected over the center of the wing on the rotor/rotor axis showing spanwise flow, fountain height, and recirculating flow. 1/2 second exposure time.

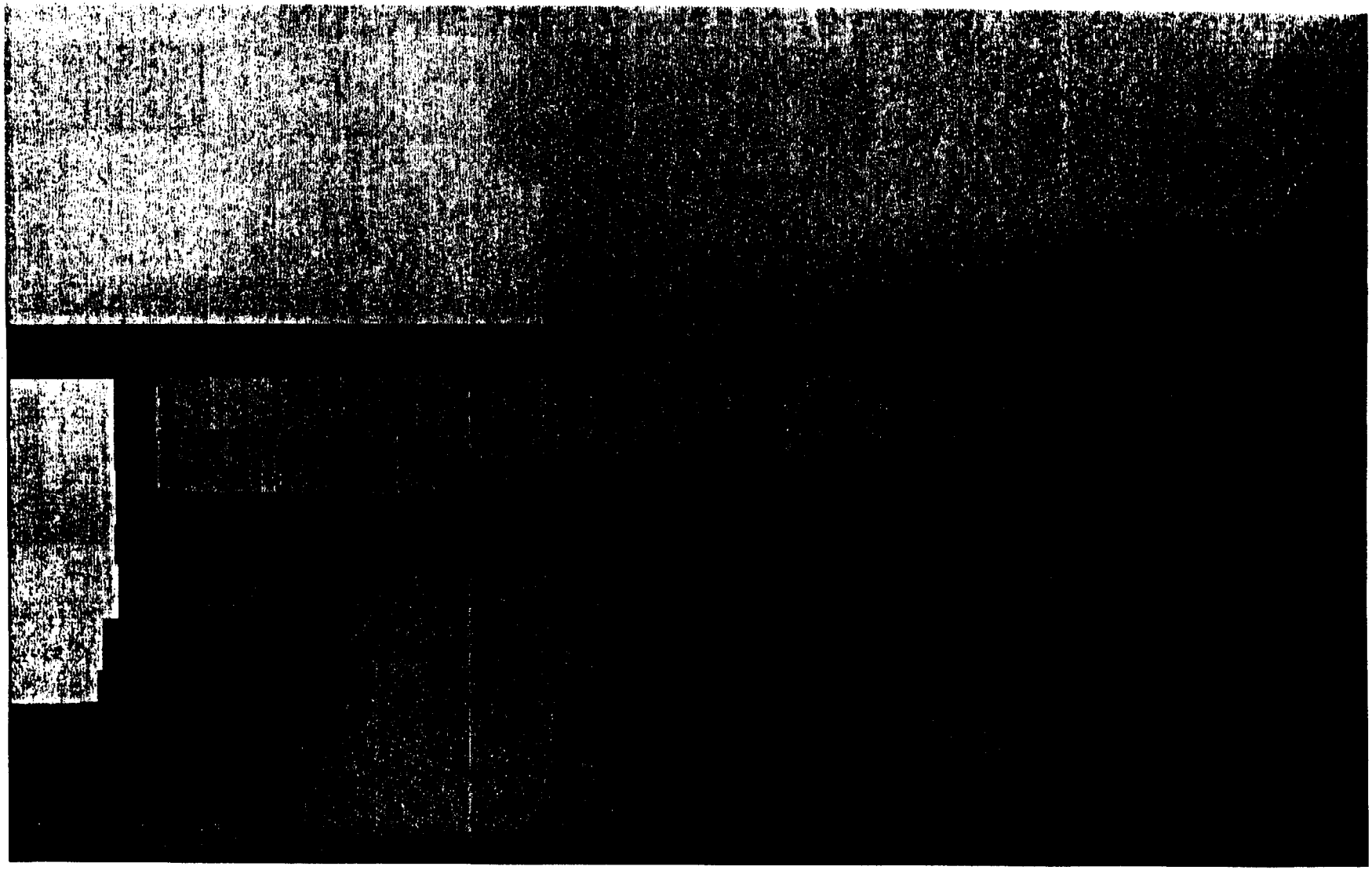

Figure 6. Computer enhanced digitized photo of fountain flow. Viewer in front of model. Bubbles are injected into the stagnation region on the center of the wing on the rotor/rotor axis showing up-flow between rotors and recirculating flow. 1/2 second exposure time.

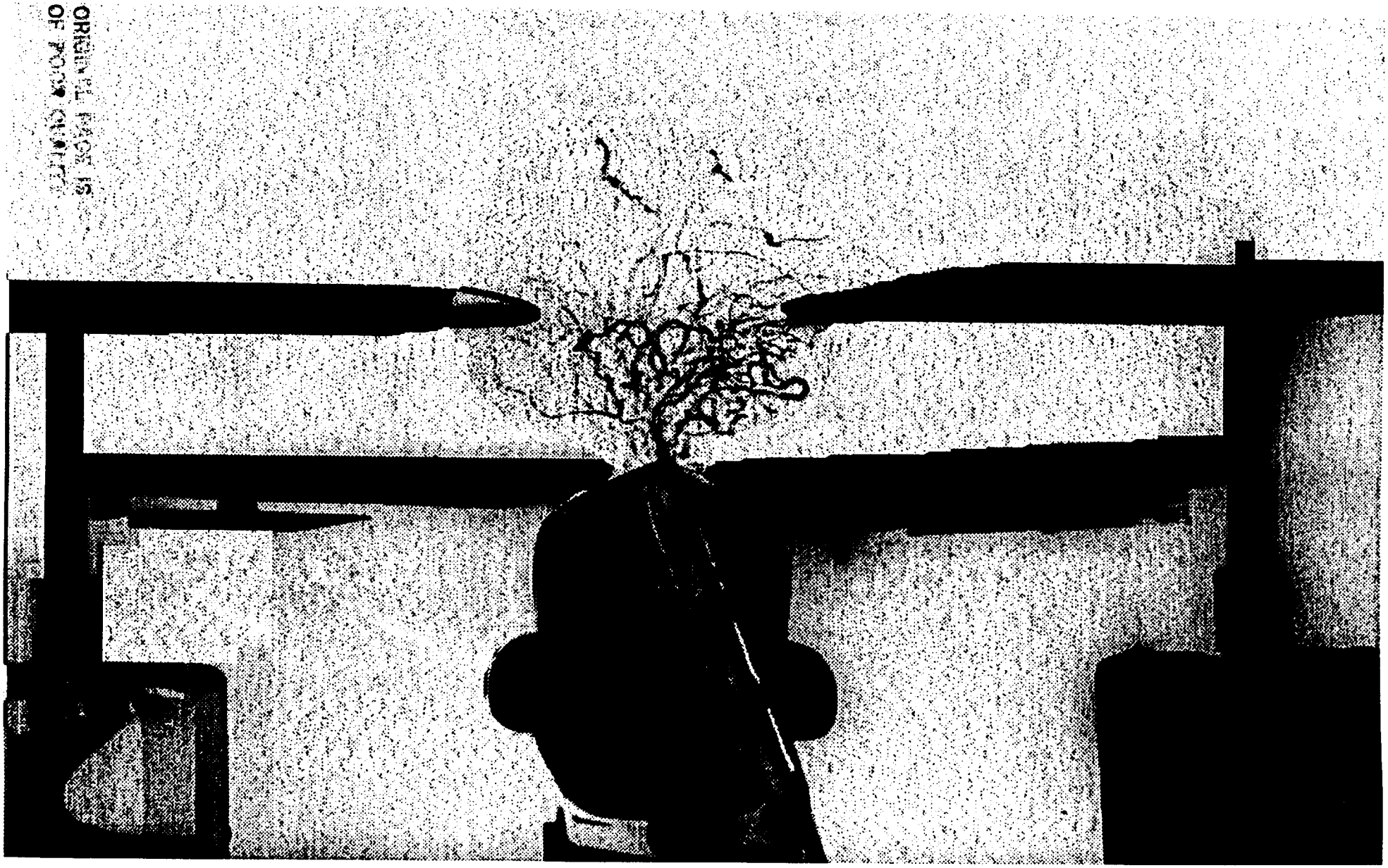

Figure 7. Computer enhanced digitized photo of fountain flow. Viewer in front of model. Bubbles are injected into the stagnation region on the center of the wing on the rotor/rotor axis showing highly turbulent up-flow between rotors and recirculating flow. 1/2 second exposure time.

Figure 8. Computer enhanced digitized photo of fountain flow. Viewer in front of model. Bubbles ar injected right of center over the rotor/rotor axis showing the unsteady asymmetric nature of the fountain. 1/4 second exposure time.

Figure 9. Computer enhanced digitized photo of fountain flow. Viewer to side of model. Bubbles are injected above rotor plane over the longitudinal axis showing the longitudinal recirculating flow. 1/2 second exposure time.

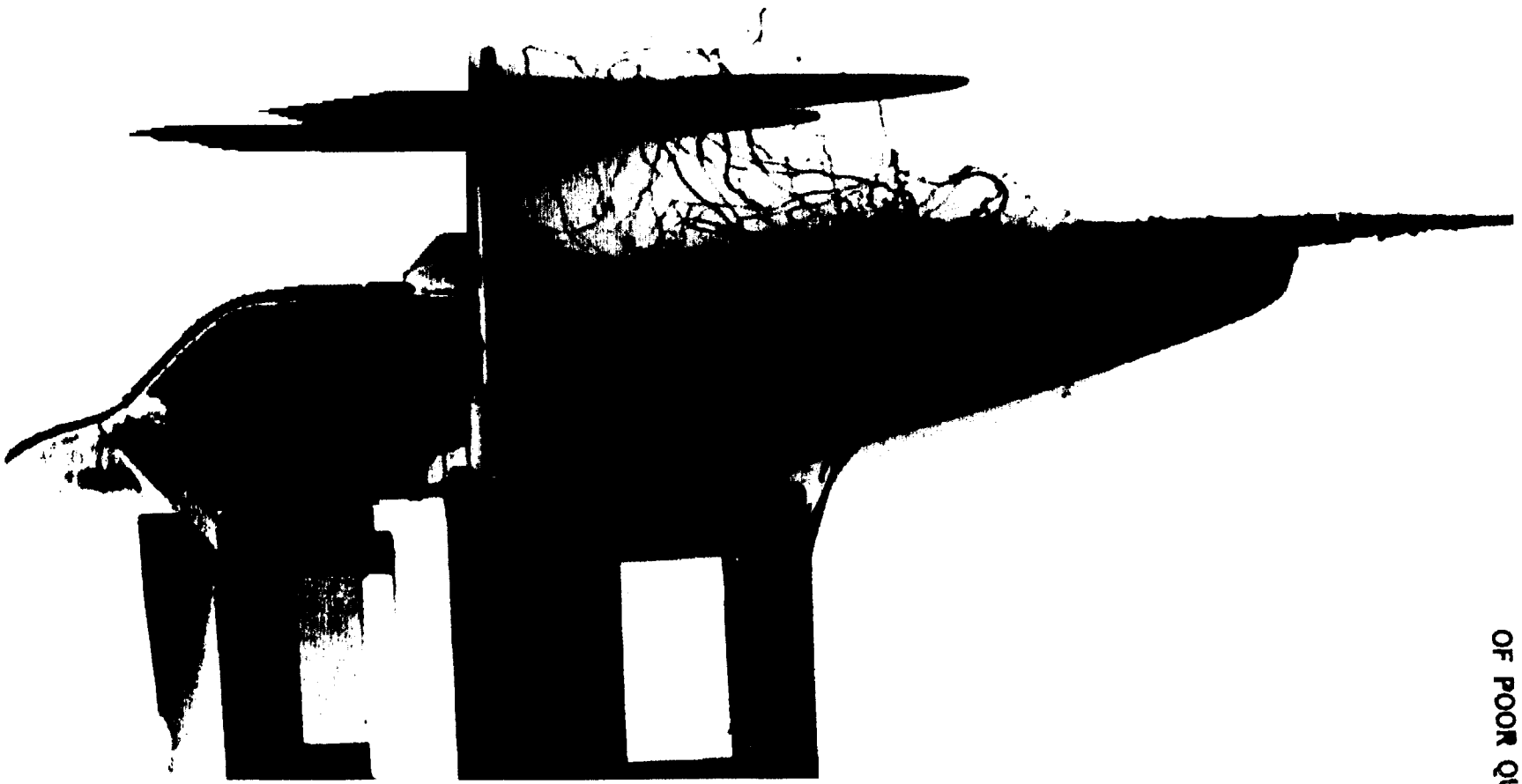

Figure 10. Computer enhanced digitized photo of fountain flow. Viewer to side of model. Bubbles are injected along the fuselage showing the turbulent up-flow over the length of the fuselage. 1/2 second exposure time.

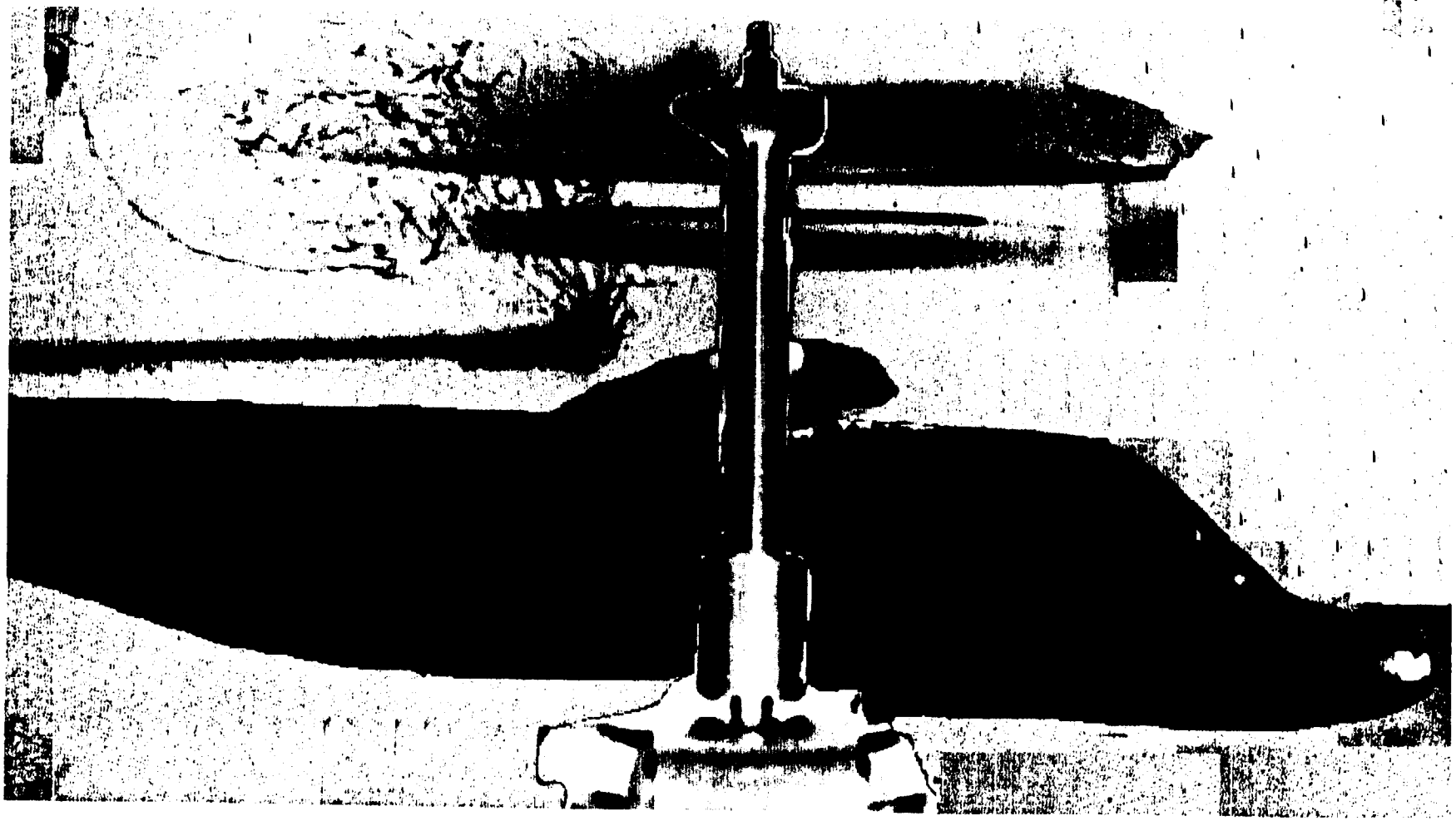

Figure 11. Computer enhanced digitized photo of fountain flow. Viewer to side of model. Bubbles are injected just above the wing on the longitudinal axis showing the recirculating flow being swept rearward.

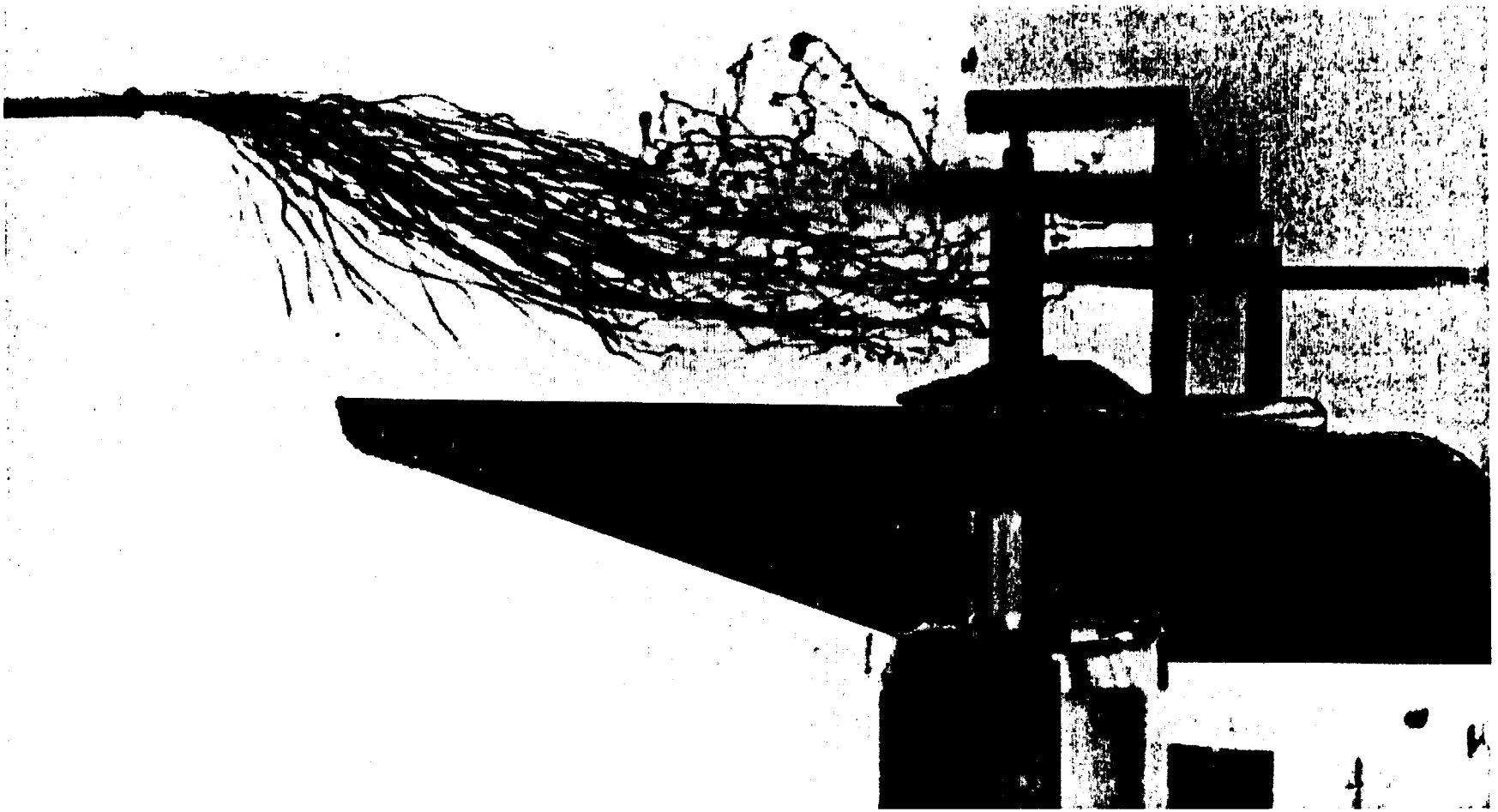

Figure 12. Computer enhanced digitized photo of fountain flow. Viewer to side of model. Bubbles are injected above the rotor plane, behind the tail and over the longitudinal axis, and show laminar inflow becoming turbulent as it encounters the fountain flow.

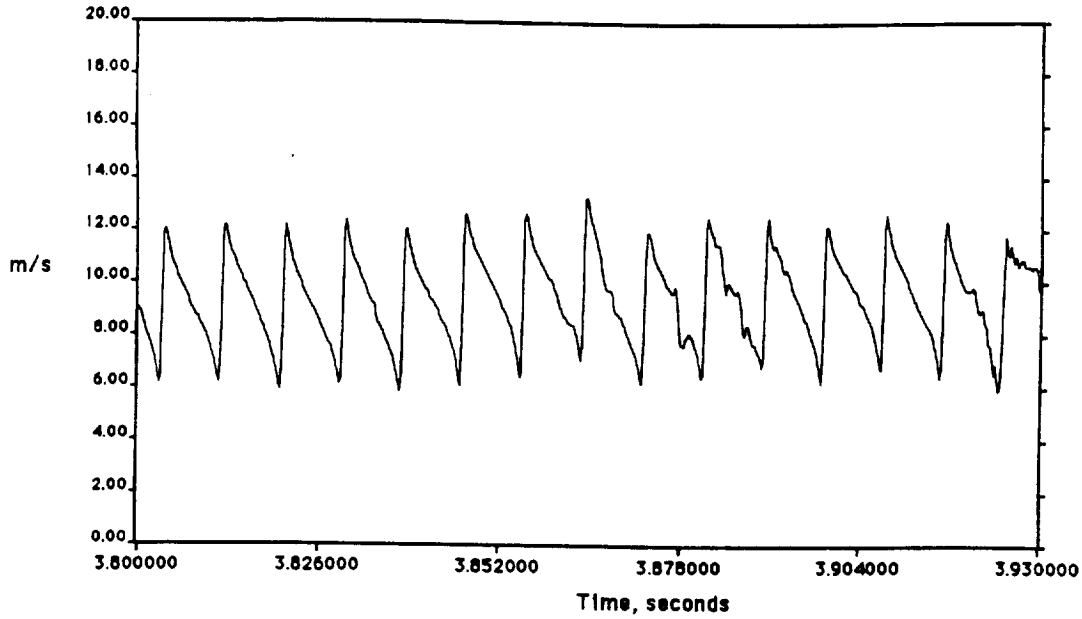

Figure 13a. Time trace of inflow velocity in the fountain re-ingestion zone showing essentially laminar flow. Data taken with the hot wire parallel to the longitudinal axis, inboard, 2 inches from the rotor tip on the rotor/rotor axis, and 1 inch above the rotor plane.

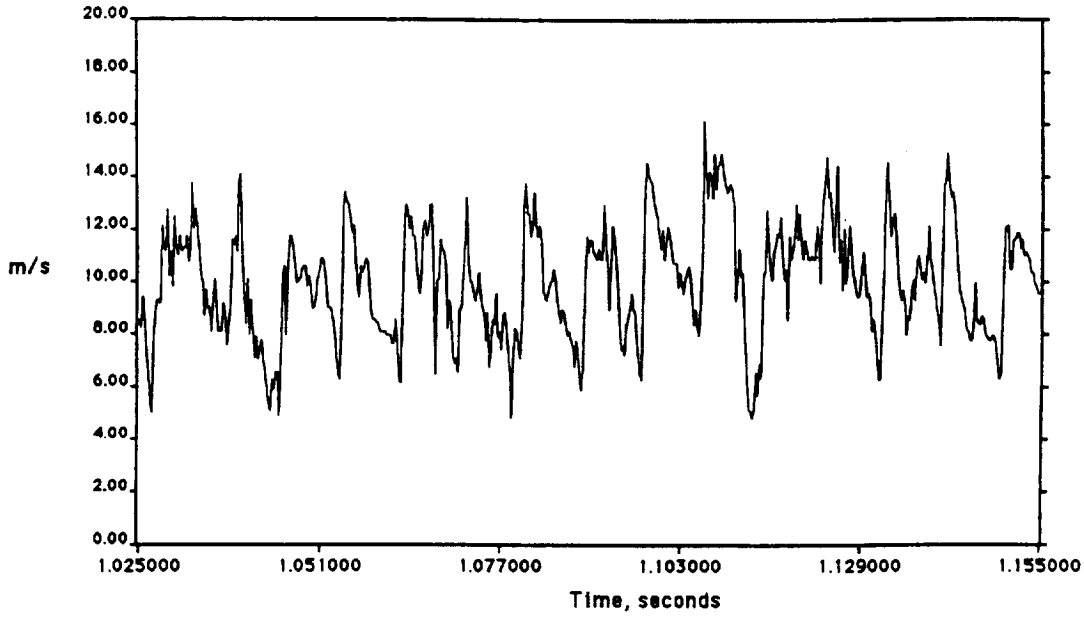

Figure 13b. Time trace of inflow velocity in the fountain re-ingestion zone showing turbulent flow. Data taken with the hot wire parallel to the longitudinal axis, inboard, 2 inches from the rotor tip on the rotor/rotor axis, and 1 inch above the rotor plane.

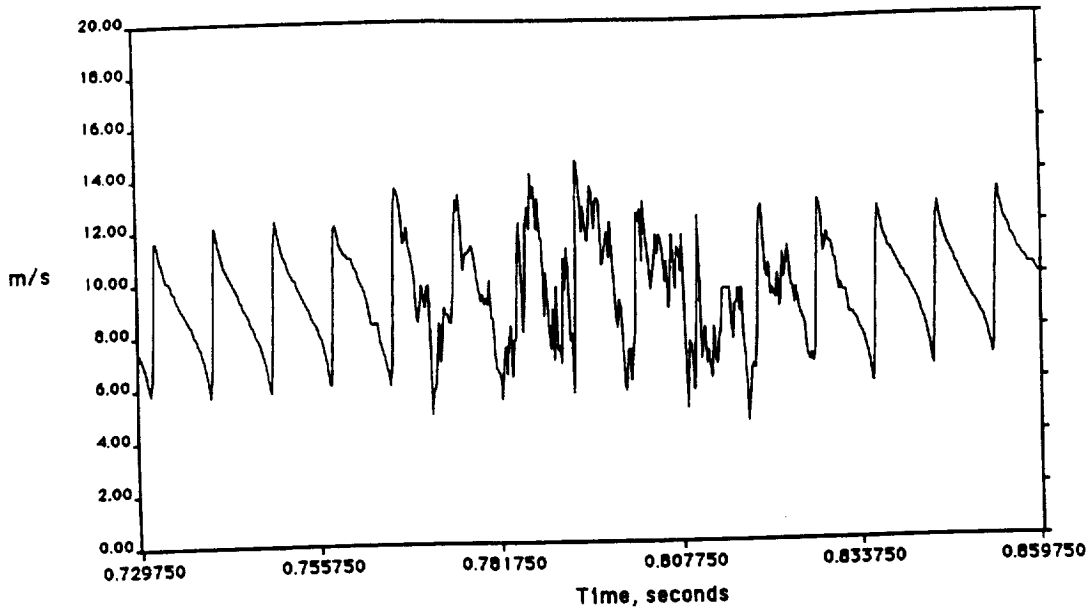

Figure 14. Time trace of inflow velocity in the fountain re-ingestion zone showing intermittently laminar and turbulent flow. Data taken with the hot wire parallel to the longitudinal axis, inboard, 2 inches from the rotor tip on the rotor/rotor axis, and 1 inch above the rotor plane.

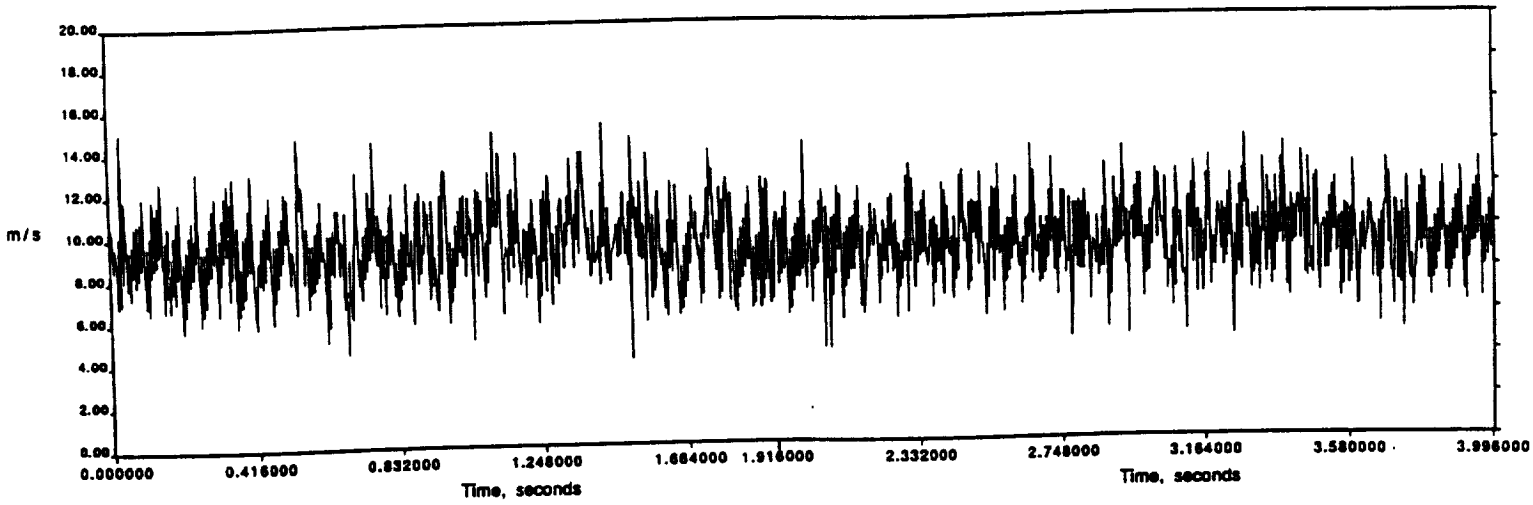

Figure 15. 4 second time trace of inflow velocity in the fountain re-ingestion zone. Data taken with the hot wire parallel to the longitudinal axis, inboard, 2 inches from the rotor tip on the rotor/rotor axis, and 1 inch above the rotor plane.

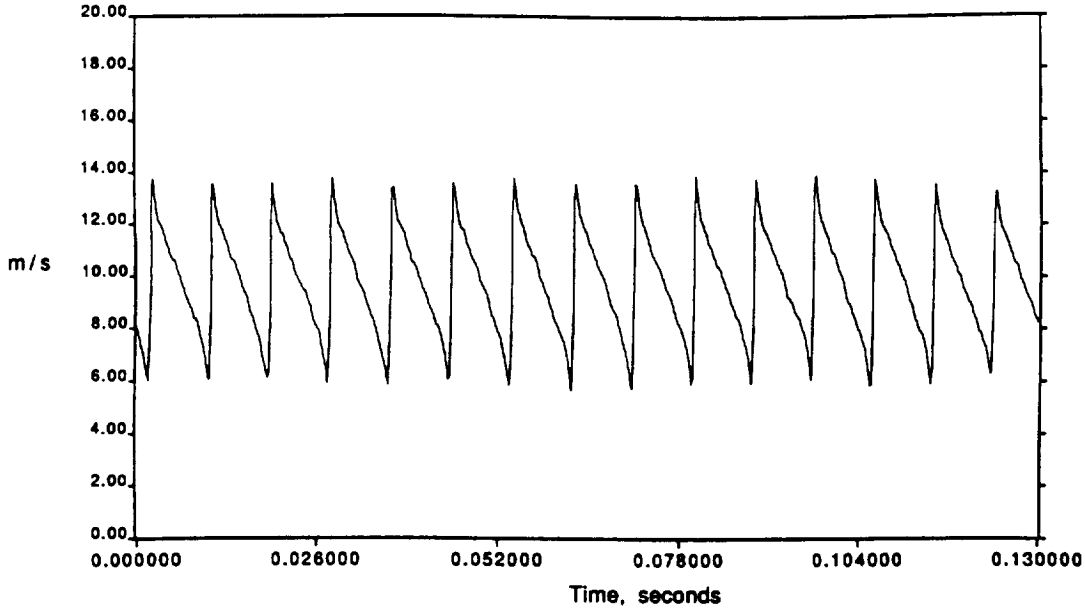

Figure 16. Time trace of inflow velocity over the outboard part of the rotor plane showing laminar flow unaffected by the fountain. Data taken with the hot wire parallel to the longitudinal axis, outboard, 2 inches from the rotor tip on the rotor/rotor axis, and 1 inch above the rotor plane.

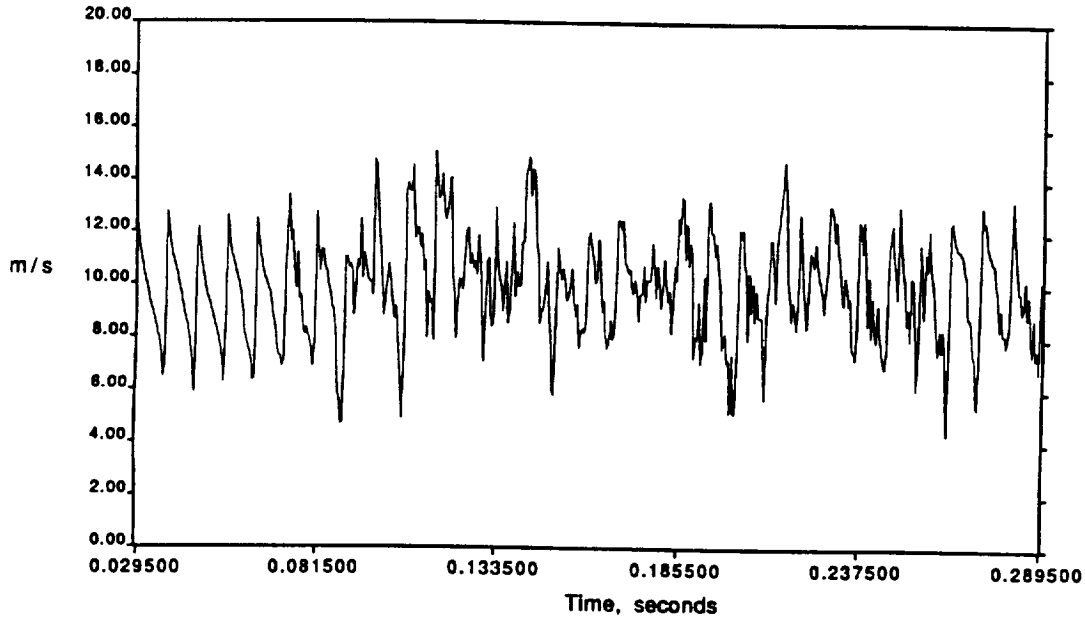

Figure 17a. 1 inch above the rotor plane.

Figures 17a-c. Time traces of inflow velocity in the fountain re-ingestion zone at different heights above the rotor plane. Data taken with the hot wire parallel to the longitudinal axis, inboard, and 2 inches from the rotor tip on the rotor/rotor axis.

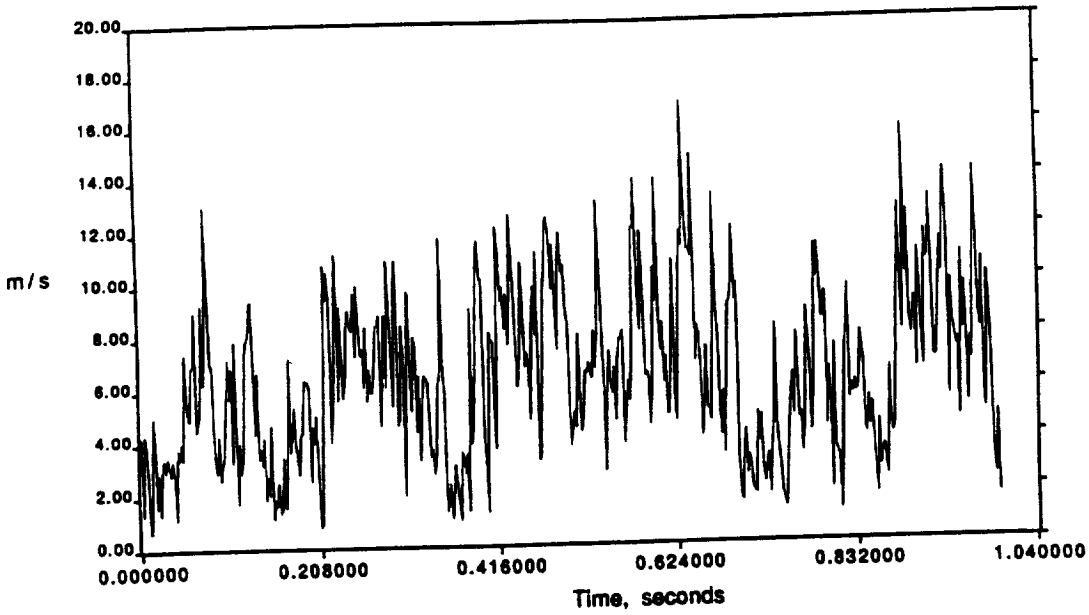

Figure 18c. Hot wire on the rotor/rotor axis.

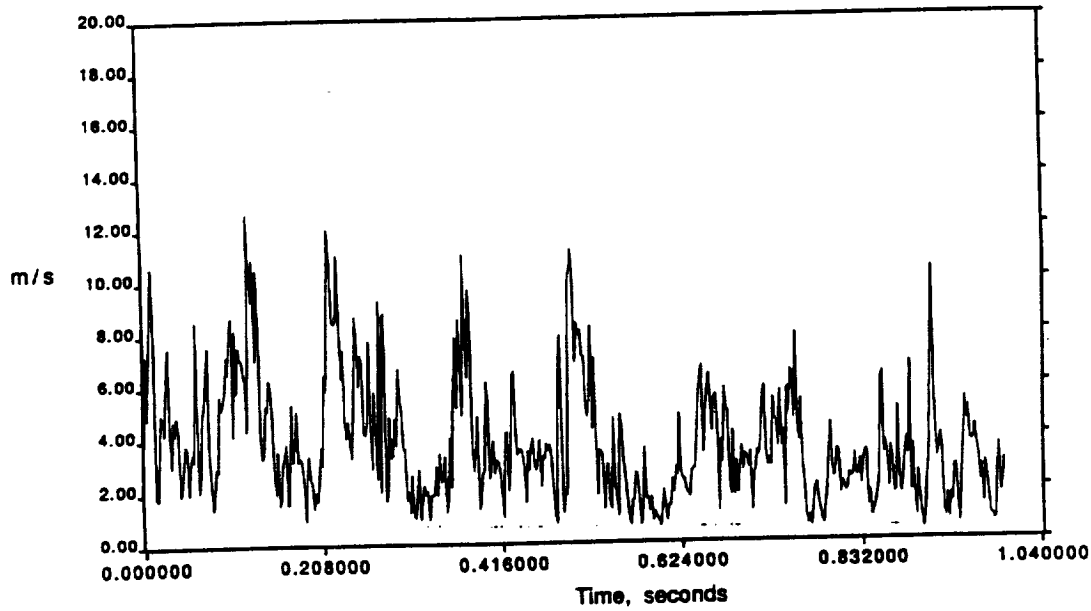

Figure 18d. Hot wire 8 inches rearward of the rotor/rotor axis.

Figures 18a-e. Time traces of velocity at locations along the longitudinal axis, 1 inch above the rotor plane. Hot wire oriented parallel to the longitudinal axis.

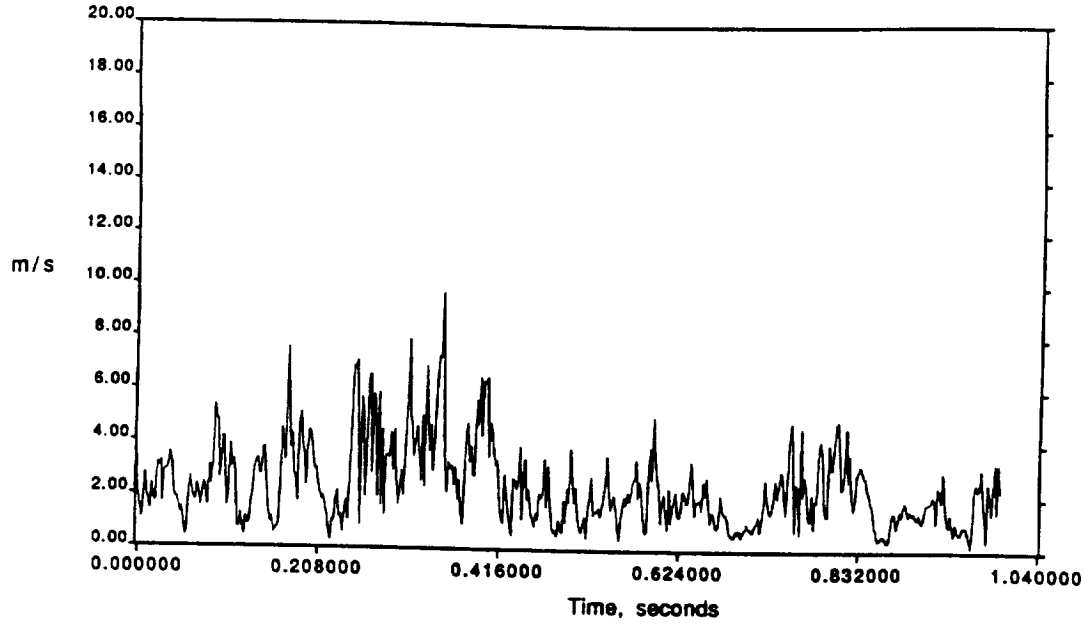

Figure 18e. Hot wire 12 inches rearward of the rotor/rotor axis.

Figures 18a-e. Time traces of velocity at locations along the longitudinal axis, 1 inch above the rotor plane. Hot wire oriented parallel to the longitudinal axis.

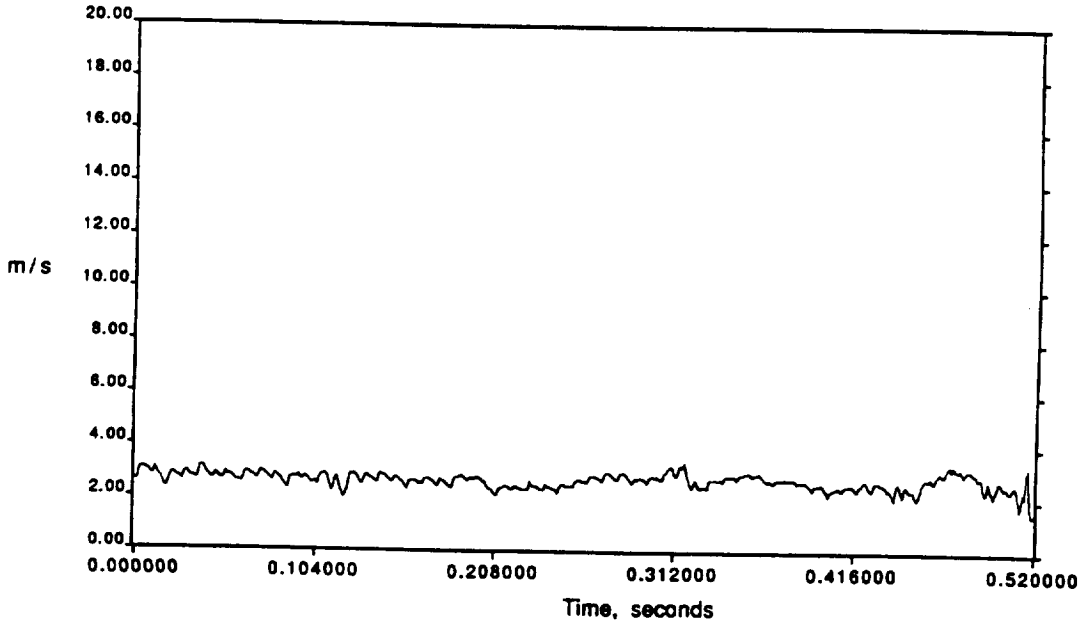

Figure 19a. One rotor spinning showing very small velocity fluctuations.

Figures 19a-b. Time traces of velocity showing the effect of one and two rotors spinning. Hot wire 1 inch above the rotor plane on the intersection of the rotor/rotor and longitudinal axis.

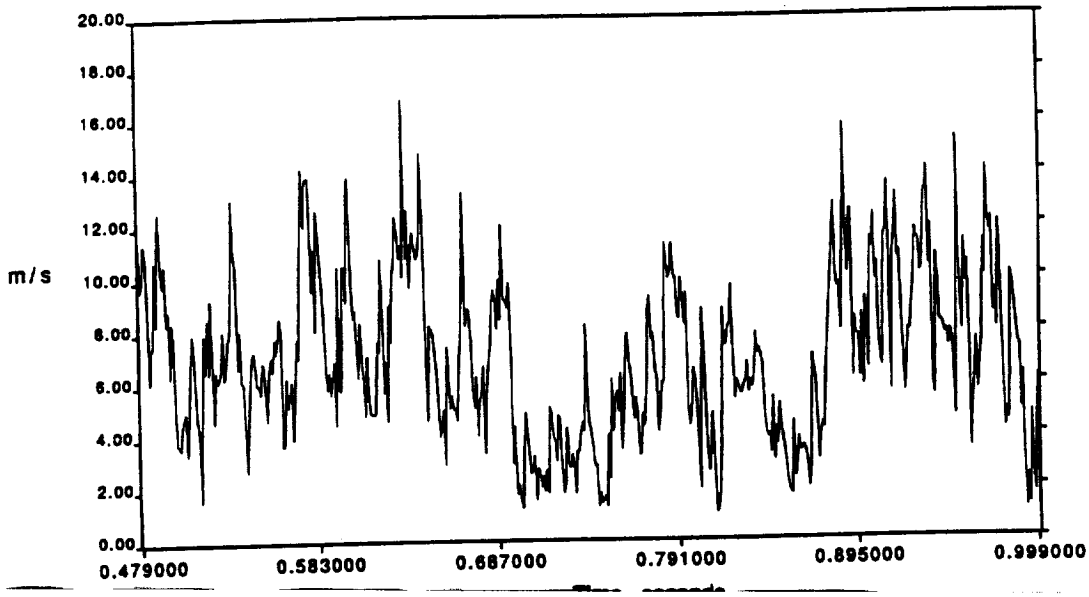
m/s
20.00
18.00
16.00
14.00
12.00
10.00
8.00
6.00
4.00
2.00
0.00
0.479000
0.583000
0.687000
0.791000
0.895000
0.999000